Revision 1

Constraints on non-isothermal diffusion modeling: an experimental analysis and error assessment using halogen diffusion in melts

Smruti Sourav Rout, Burkhard C. Schmidt, Gerhard Wörner
Geowissenschaftliches Zentrum, Georg-August-Universität (GZG),
Goldschmidtstrasse 1, 37077 Göttingen, Germany
Email: srout@geo.uni-goettingen.de
Phone: +4917636504483

Abstract

Diffusion chronometry on zoned crystals allows constraining duration of magmatic evolution and storage of crystals once temperatures are precisely known. However, non-isothermal diffusion is common in natural samples and thus, time-scales may not be determined with confidence while assuming isothermal conditions. The “Non-isothermal Diffusion Incremental Step (NIDIS) model” (Petrone et al. 2016) is proposed for such cases for a non-isothermal diffusive analysis. We conducted diffusion experiments with stepwise temperature changes to analyze and test the model, evaluated the associated errors and improved the accuracy by suggesting an alternative algorithm to model diffusion times.

We used Cl and F (≤0.4 wt.%) as the diffusing elements in nominally anhydrous (H_2O≤0.3 wt.%) phonolitic melt with composition of Montana Blanca (Tenerife, Spain) in an experimental set-up that successively generates multiple diffusive interfaces for different temperatures by adding glass blocks of different Cl and F concentrations. This compound set of two diffusion interfaces represents distinct compositional zones that diffusively interact at different temperatures, which can be taken as an equivalent to non-isothermal diffusion in zoned magmatic crystals. The starting temperature ranged from 975 to 1150 °C and each set of experiments included a temperature change of 85-150 °C and a total duration of 8-12 hours. The experiments were carried out in an internally heated pressure vessel equipped with a rapid quench device at 1 kbar pressure. Cl and F concentration profiles were obtained from the quenched samples by electron microprobe analysis. Although the estimated diffusion times from the NIDIS-model matched well with true experimental values, the errors on estimated time-scales, accounting for errors in curve-fitting and uncertainty in temperature, were ±10-62% (1σ). The errors are much larger at 61-288% (1σ) when the uncertainty in diffusivity parameters is included. We discuss the efficiency and limitations of the model, assess the contribution from different sources of error, and their extent of propagation. A simpler alternative algorithm is proposed that reduces errors on the estimates of diffusion and residence time to 10-32% (1σ) and 60-75% (1σ), with and without including uncertainty in diffusivity parameters, respectively. Using this new algorithm, we recalculated the individual diffusion times for the clinopyroxene crystals analyzed by Petrone et al. (2016) and obtained a significantly reduced error of 26-40% compared to the original error of 61-100%. We also analyzed a sanidine megacryst from Taapaca volcano (N. Chile) as a test case for non-isothermal modeling and obtained diffusion times of 1.5 – 9.4 ky, which is significantly different from isothermal analyses including a previous study on similar sample. In this analysis, the error estimated by our new method is reduced by 63-70%.

Keywords

Non-isothermal diffusion, Diffusion experiment, Error assessment, Electron microprobe, Halogen diffusion

Introduction

The pre-eruptive history of magmas at active and potentially dangerous volcanoes is archived in the compositional zonation in magmatic crystals. These zonations record the nature and rates of magmatic processes and the time-scales of magma storage prior to eruption. In the past decades, petrographic and compositional analysis of minerals have allowed volcanologists a better comprehension of storage conditions and storage periods of magma as well as the nature and timing of eruption triggering events (e.g. Reid 2003; Hawkesworth et al. 2004; Morgan and Blake 2006; Cooper and Kent 2014; Rubin et al. 2017). Minerals that crystallize from a melt over the course of time record any changes in the crystallizing conditions (temperature, pressure, oxygen fugacity; e.g. Holland and Blundy 1994; Johnson and Rutherford 1989; Ridolfi et al. 2010) and melt composition (e.g. Ginibre et al. 2007; Ruprecht and Wörner 2007; Chakraborty 2008; Costa and Chakraborty 2004; Morgan and Blake 2006; Costa and Morgan 2010). Two methods are employed to extract information on time-scales of crystallization and magmatic processes. One is the direct dating of crystals using short-lived U-series isotopes (e.g. Condomines et al. 1988; Hawkesworth et al. 2000; Hawkesworth et al. 2004; Schmitt 2011) that provides insights into their time of formation and thus, gives minimum values for the age and storage duration of magmas. For example, ^{230}Th-^{226}Ra dating applied to Santorini (Zellmer et al. 2000) and Kilauea Volcano, Hawaii (Cooper et al. 2001), and U-Th-Ra disequilibria applied to MORB and OIB (Condomines et al. 1988) constrain time-scales of fractional crystallization, magma transport and residence up to 10^5 years. A second approach to estimate residence time and ages of crystals is based on diffusion speedometry of zoned phenocrysts which has been applied, for example, to plagioclase (Zellmer et al. 1999; Costa et al. 2003), pyroxene (Morgan et al. 2004; Chamberlein et al. 2014), olivine (Costa and Dungan 2005; Costa and Chakraborty 2004), quartz (Chamberlein et al. 2014; Ackerson et al. 2018) and sanidine (Zellmer and Clavero 2006; Chamberlein et al. 2014; Iovine et al. 2017).

These studies assumed isothermal conditions during diffusion and thus a constant diffusion coefficient. However, under natural conditions, temperatures may vary throughout the growth of a crystal (Costa et al. 2008). Such variation is often associated with magma mixing, or magma transport that lead to compositional zonation in the crystal (Morgan et al. 2004; Watson and Müller 2009; Chakraborty 2008; Costa and Chakraborty 2004) and is shown by distinct dissolution interfaces and regrowth events that clearly indicate temperature variations of 100 °C or more (e.g. Ginibre et al. 2004, Cooper and Kent 2014). In earlier diffusion studies, lack of constraints on intra-crystal temperature variations allowed only isothermal modeling of diffusion boundaries. Many cases consider only the final resorption-growth event and this should give meaningful results for calculated diffusion times using a single temperature value (e.g. Chamberlein et al. 2014 and our own study of the Campi Flegrei, Italy, Iovine et al. 2017). In these and many other cases only a single zone boundary was analyzed for a fixed temperature. In other cases, when there was no constraint to account for possible temperature variation during growth, the potential information that can be gained from multiple diffusion zones that developed during the larger part of a crystal's history is limited. In such cases, isothermal diffusion modeling of multiple growth and diffusion gradients will not yield robust time-scales and a non-isothermal diffusion modeling is necessary. And In order to apply non-isothermal diffusion modelling it is vital to know the temperature-time history of the crystal.

Lasaga (1983) already addressed the issue of the non-isothermal nature of diffusion in minerals and suggested methods to model diffusion during consistent cooling intervals. Similar cooling models have been used by other studies to constrain diffusion in minerals of high-grade metamorphic rocks (Ganguly et al. 2000), martian meteorite (Bloch and Ganguly 2014), cooling lavas (Gardner et al. 2012; Befus et al. 2015), lunar glasses (Saal et al. 2008), and granites (Ackerson et al. 2018). However, for magmatic environments, where crystals undergo frequent heating, cooling and growth events at various amplitude and frequencies (Ginibre et al. 2007; Cooper and Kent 2014; Rubin et al. 2017), applying non-isothermal analysis is a challenge. Ideally, the temperature associated with each growth zone is needed for precisely constraining the time-scales and frequency of magmatic processes that form the zonation, as well as for estimating the total residence time.

To address diffusion in more complex magmatic crystals, Petrone et al. (2016) suggested a “Non-isothermal diffusion incremental step (NIDIS) model” to obtain diffusion time-scales from different zone boundaries that formed at different temperatures within a single crystal. The model uses different diffusion coefficients for different diffusive boundaries according to different temperatures for the corresponding zones. Thus, it is possible to extract information from all diffusive boundaries unlike the usual isothermal analysis where only the outer-most boundary gives robust information. Petrone et al. (2016) used the model to constrain the residence history of compositionally zoned clinopyroxene crystals from Stromboli volcano (Italy) from the present-day activity (<2000 years). In this study, we test the accuracy of this model through a series of controlled experiments, ground-truth the model by analyzing the associated errors and give a simpler yet relatively more accurate alternative mechanism to use the non-isothermal diffusion model using the underlying basic concept.

Non-isothermal diffusive analysis and the NIDIS model:

The diffusion coefficient (D) is strongly dependent on temperature (T) and varies exponentially through the Arrhenius equation (Eq 1):

$$D = D_0 e^{\frac{-E_A}{RT}} \tag{1}$$

where E_A (J/mol) is the activation energy, R [8.3145 J/(mol·K)] is the universal gas constant, D_0 (m^2/s) is the pre-exponential factor and corresponds to the value of D (m^2/s) at infinite temperature and T is the temperature in Kelvin. Petrone et al. (2016) suggested a backward model in which the diffusion time associated with individual diffusive boundaries can be constrained. For this model to work, the parameters in Eq 1 (E_A and D_o), that are used to calculate diffusion coefficient (D) for different temperatures, have to be known. In total, four conditions need to be fulfilled: (1) concentration and temperature independent D_0 and E_A, (2) one-dimensional diffusion in a semi-infinite medium (as reported by Crank 1975), (3) periods between temperature changes are isothermal, (4) duration of temperature change between the isothermal periods is negligible. However, in the later sections, we present a method of using the model when condition 3 and 4 from above are not satisfied.

To explain the model, we use the simple case of a crystal with three growth zones of different composition that were formed at different temperatures (Fig 1) which are known. Following the core of the crystal, the mantle is formed at a temperature T_1. T_1 is maintained until the rim of the crystal is formed after some time at temperature T_2. T_2 is maintained until eruption. The time interval between the formation of the mantle and the rim is t_1 whereas the interval between formation of rim and closure of diffusion is t_2. The term “closure” is used for the condition when temperature drops to a particular value below which diffusion is negligible (known as closure temperature). In this case the closure of diffusion will be at the moment of eruption when the temperature drops below closure temperature. In the above case, the core-mantle boundary in a crystal undergoes diffusion for a duration of t_1 at temperature T_1 and then again for t_2 amount of time at temperature T_2, whereas the mantle-rim boundary undergoes diffusion only for the duration of t_2 at temperature T_2. The Petrone et al. (2016) model operates backwards starting from the rim and ending at the core. For the mantle-rim boundary, the diffusion time t_2 is obtained by applying a curve-fitting to the concentration profile using the diffusion coefficient D_2 for temperature T_2 (see “Results and discussion” below for curve fitting details). Then an imaginary timescale t_3 is obtained for the same profile using the diffusion coefficient D_1 for the temperature T_1. This imaginary time-scale t_3 is the duration one would get if the mantle-rim boundary diffused entirely at temperature T_1 instead of T_2. Then, the core-mantle boundary is assumed to have diffused only at T_1 and thus is modeled for T_1 to give a second imaginary time-scale t_4 (using D_1). The difference between t_4 and t_3 is t_1 which is the actual diffusion time at the core-mantle boundary at T_1. The sum of t_1 and t_2 gives the total residence time of the crystal.

Alternative curve parameter method:

Mathematically (see below), the above steps are equivalent to arithmetically operating the corresponding products of diffusion coefficient (D) and time (t), Dt. Here onwards, we refer to Dt, which is specific to each diffusion profile, as ‘curve parameter’.

Let the curve parameter for core-mantle boundary (profile 1) and mantle-rim (profile 2) be CP_1 and CP_2 respectively. Temperature values are T_1 and T_2 and corresponding diffusion coefficients are D_1 and D_2 respectively. The durations to be obtained are t_1 and t_2, where t_2 is the diffusion time after the mantle-rim boundary (profile 2) was formed and t_1 is the diffusion time of core-mantle boundary (profile 1) before mantle-rim boundary (profile 2) started to form.

As per NIDIS model by Petrone et al. (2016), $t_2 = \frac{CP_2}{D_2}$.

Then, the fictional time scale t_3 and t_4 are obtained as $t_3 = \frac{CP_2}{D_1}$ and $t_4 = \frac{CP_1}{D_1}$;

Finally, t_1 is obtained by subtracting t_3 from t_4.

Thus, $t_1 = t_4 - t_3 = \frac{CP_1}{D_1} - \frac{CP_2}{D_1} = \frac{(CP_1 - CP_2)}{D_1}$

From the above equation, $D_1 t_1 = CP_1 - CP_2$ (2)

Thus, instead of following the steps of NIDIS model as given in Petrone et al. 2016, t_1 can directly be obtained by taking the ratio of (1) the difference in curve parameters of the profiles of core-mantle and mantle-rim boundary i.e. ($CP_1 - CP_2$) and (2) the corresponding diffusion coefficient (D_1, obtained using T_1). The curve parameter for each profile can be easily obtained from the curve fitting.

This illustrates the underlying concept behind the model where the curve parameters are arithmetically added for a particular diffusive boundary as the temperature changes through the course of diffusion. Thus, if a diffusive boundary has undergone temperatures T_1, T_2, T_3 ...T_n. for durations t_1, t_2, t_3 ...t_n respectively, then the final curve parameter (Dt) for that diffusive boundary would be a summation of all individual curve parameters (D_1t_1, D_2t_2, D_3t_3 ...D_nt_n) from all growth intervals of the crystal. Mathematically, the final Dt = $\Sigma D_n t_n$. The advantage of this set of calculation steps is that the uncertainty in temperature contributes only once to the initial time-scale t_1 as well as to every successive time-scale. This is in contrast to the algorithm given by Petrone et al. (2016), where the uncertainty in temperature contributes more than once as the time-scale for every boundary other than the outer-most boundary are obtained using imaginary time-scales which are individually calculated using temperature data. Both calculation models assume that all interfaces between the growth zones were initially perfect compositional step functions. When applying this to natural crystals where growth zones are separated by resorption interfaces, this is a valid assumption.

In this study, we tested the reliability and accuracy of the NIDIS model by experimentally generating a series of compositional interfaces at different temperatures between melts of constant major element composition but with different Cl and F concentrations. Diffusion gradients that had formed during the experiment at variable consecutive temperatures were measured by electron microprobe across the diffusive interfaces and were analyzed and modeled with the NIDIS algorithm given by Petrone et al. (2016) and the alternative algorithm given in this study. The errors originating from both of the algorithms were compared.

Experimental and analytical techniques

Starting material:

For our experiments, we used a glass of the composition of the Montana Blanca phonolite (MBP) (Table 1) with different concentrations of Cl and F as the diffusing elements. The range of diffusion coefficients for Cl and F lies between $2x10^{-14}$-$5x10^{-13}$ m^2/s and $5x10^{-13}$-$4x10^{-12}$ m^2/s, respectively in the temperature range 900-1200 °C (Böhm and Schmidt 2013), resulting in diffusion that is fast enough to perform experiments within a day and to obtain diffusion profiles with compositional and spatial variations that can be well resolved by electron microprobe. Cl and F diffusion is also independent of their concentration (Dingwell and Scarfe 1984; Alleti et al. 2007; Balcone-Boissard et al. 2009) making it easy to analyze the profiles for diffusion modelling. Böhm and Schmidt (2013) have constrained F and Cl diffusion coefficients in nominally dry and hydrous (2.1-2.4 wt%) Montana Blanca phonolitic (MBP) melt for 800 to 1200 °C, thus making it a suitable medium to carry out our non-isothermal diffusion experiments.

For the anhydrous halogen-free starting glass, six different oxides (SiO_2, Al_2O_3, Fe_2O_3, TiO_2, MnO_2, MgO) and three carbonates (Na_2CO_3, K_2CO_3, $CaCO_3$) were mixed together. This mixture was then put into a platinum crucible and was first decarbonated in air at 1000 °C and then melted in an oven at 1600 °C and 1 atm pressure. After 30 minutes the melt was quenched to glass by dipping the bottom of the crucible into cold water. A short melting time of 30 min was maintained to minimize Na loss. To obtain a homogenized composition, this glass was ground up to a powder which was again melted. This process was repeated twice.

Glasses with about 0.4 wt% Cl and 0.4 wt% F were prepared separately. Cl-rich glass was prepared by adding NaCl and F-rich glass was prepared by adding NaF to the to the halogen free MBP glass powder. About 1 g of each of these mixtures was sealed inside $Au_{75}Pd_{25}$ capsules (35 mm length, 6 mm outer diameter, 0.2 mm wall thickness), welded shut, pressurized with water for 16 hours in a hydrothermal autoclave to check for possible leaks, and then melted at 1200 °C and 1.5 kbar pressure for 120 hours in an internally heated pressure vessel (IHPV) to produce bubble free halogen-bearing glass cylinders. The cylinders were cut and polished (down to 1 µm) to rectangular glass blocks of 20x4x1.4 mm. Smaller rectangular blocks of 4x1.6x1.4 mm were cut out of these large glass blocks using a diamond saw. These blocks are used as individual units in creating diffusive interfaces.

The water contents of the glasses were determined by mid-infrared (MIR) Fourier transform (FT) spectroscopy using a Bruker Vertex 70 spectrometer with attached IR microscope Hyperion 3000. The water content for all the samples was between 0.2 and 0.3 wt%. The anhydrous MBP glass used by Böhm and Schmidt (2013) also contained up to 0.3 wt% of water. Thus, the diffusivity values given by Böhm and Schmidt (2013) are applicable here without any modifications.

Experiments:

Each F-rich glass block was paired with a Cl-rich glass block and the assemblage was wrapped in a thin Pt foil (0.05 mm thickness), welded shut in a Pt cylinder (0.2 mm thickness, 4 mm outer diameter and 15 mm length), and pressurized for 1 hour in a cold seal pressure vessel. The Pt-sheet wrapping and the pressurization ensured a tight contact between the glass blocks across their 1.6x1.4 mm polished surfaces.

The IHPV was also used for the diffusion experiments. It operated vertically and was equipped with a rapid quench mechanism similar to that of Roux and Lefèvre (1992). The sample capsules were placed in a Pt sample holder that was suspended from a Pt quench wire (0.125-0.15 mm diameter) connected to two electrodes. To avoid internal convection, the capsules were placed in a manner so that the Cl-rich part would be at the bottom. During the experiment, the suspended sample holder was located in the hot spot zone of the furnace, where the thermal variation could be minimized to less than 5 °C by adjusting the two platinum windings of the furnace. Temperature was recorded by three S-type thermocouples at ±5 °C accuracy. Pressure was maintained by compressing Ar and recorded by a transducer, calibrated (to ±50 bars) against a Heise tube gauge. Heating was isobaric at 40±2 °C/min by constantly increasing the output power over time. Using this procedure, the heating to the final temperature took between 20 and 30 min. Quenching was much faster by fusing the quench wire electrically, which makes the sample drop into the cold bottom part of the vessel (T<50 °C). The cooling rate in similar experiments was determined to be ~150 °C/s by Benne and Behrens (2003).

The experimental set-up was designed to successively create multiple diffusive interfaces (Fig 1). At first, a diffusion couple is heated to a temperature T_1 (Fig 1a) and maintained at T_1 for t_1 amount of time (Fig 1b) and then, rapidly quenched. A second diffusion couple is then added and both couples are heated to another temperature T_2 (Fig 1c) and maintained for a different duration of t_2. Both couples are then rapidly quenched at the end of t_2 (Fig 1d) which marks the closure of diffusion. Fig 2a shows an example (experimental set 1) of the two capsules recovered at the end of t_2 in one experimental set. The temperature for each experiment varied from 975 to 1150 °C and duration (run time) for each experiment was between 3 to 7 hours. The samples were recovered to be analyzed for diffusion profiles. The heating and diffusion times were chosen so that the diffusion gradients will remain significantly shorter than the half-size of each glass block of the diffusion couples. This allows us to take the two couples as part of the same system where they represent two successive zone boundaries in a crystal. A total of 3 sets of experiments i.e. 6 individual experiments were performed. The diffusion times considered (t_1, t_2) are the duration at which the target temperature was maintained, which excludes the duration of heating and cooling. However, diffusive exchange during heating (40°C/min) and cooling (150 °C/s) is small and was corrected for (see below). Experimental conditions of all experiments are listed in Table 2. We used different run durations and temperatures after introducing the second glass sample. Compared to T_1, the temperature during t_2, i.e. T_2, was increased for set 3 and decreased for sets 1 and 2. This was done keeping in mind that in magmatic systems the storage temperature for crystals can either increase or decrease after magma mixing. For example, in the case of a hot mafic recharge, the change in temperature for a crystal residing in colder silicic magma is positive while in the case of a crystal which comes up with the mafic magma that mixes with the shallow colder magma, the change in temperature is negative.

Analytical techniques:

After the termination of the entire experiment, the quenched samples were cut parallel to the diffusion direction at 90° across the interface between the halogen-rich and halogen-poor blocks and embedded in epoxy resin to be polished for electron microprobe (EMP) analysis (Fig 2a). F and Cl concentrations were measured together with major elements except oxygen through line analysis across the diffusive boundaries. The lines were set perpendicular to the diffusive interface. Fig 2b shows an example of a measured sample (capsule 1 of experimental set 2) in back scattered electron (BSE) image with the former interface and a series of points from quantitative analysis. All analyses were performed with a JEOL JXA 8900 RL at an acceleration voltage of 15 kV, a beam current of 15 nA, and a beam diameter of 20 and 25 µm. Major elements were measured with a dwell time of 15 s on the peak and 5 s on the background. F and Cl were measured with a dwell time of 30 s on the peak and 15 s on the background. Topaz was used as a standard for F, synthetic NaCl for Cl, albite for Na, sanidine for K, hematite for Fe, olivine for Mg, wollastonite for Ca and Si, synthetic rutile for Ti, rhodonite for Mn and anorthite for Al. The detection limits for Cl and F are ~50 ppm and ~180 ppm respectively. The relative standard deviation (1σ) for Cl and F were <5% and <10%. Analytical data for the experimental sets are presented in supplementary material 1.

EMP measurements were also done on the amphibole inclusions used for thermometry in the sanidine megacryst studied as an application of the model to natural sample. 15 KV accelerating voltage, 15 nA beam current and 10 µm beam size were used. Counting times for all the elements were 15 sec on the peak and 5 sec on the background. Calibration standards were olivine for Si and Mg, albite for Na, anorthite for Al, sanidine for K, hematite for F, TiO_2 for Ti, Wollastonite for Ca, Cr_2O_3 for Cr, Rhodonite for Mn and NiO for Ni. The relative standard deviation for major oxides was below 5% and the absolute error calculated for minor oxides was between 0.003 and 0.03 wt%. Accumulated back scattered electron (BSE) images were acquired in COMPO mode with 20 kV accelerating voltage and 20 nA beam current with a slow scanning beam with acquisition time of 120 sec per accumulation. Data from these measurements are presented in supplementary material 2.

Results and discussion:

Estimating diffusion times in non-isothermal diffusion analysis:

A least square fitting (with Chi-squared goodness of fit) was applied to model the halogen diffusion profiles (examples given in Fig 3) obtained from EMP analysis to extract the fitting parameters (√(4Dt)) and corresponding curve parameters (Dt) for individual profiles. Eq 3 was used as the solution for the diffusion profiles (Crank 1975)

$$C(x,t) = \frac{(C_{high}+C_{low})}{2} - \frac{(C_{high}-C_{low})}{2} \times \mathrm{erf}\left(\frac{(x-x_0)}{\sqrt{4Dt}}\right) \quad (3)$$

where C(x,t) is the halogen concentration (wt%) at position x after time t (s, experimental duration). C_{low} is the initial halogen concentration in the halogen-poor block and C_{high} is the initial halogen concentration at the halogen-rich block, D is the diffusion coefficient (mm^2/s) and x_0 (mm) is the position (x-coordinate) of the diffusive interface.

Calculations were done using diffusivity data from Böhm and Schmidt (2013) and the two methods (the algorithm from Petrone et al. (2016) and the alternative curve parameter method) described earlier. These diffusion time estimates (see Table 3) can be compared to the durations of diffusion in the experiments. The calculated durations from the two methods, as expected, were exactly the same and thus, only one set of calculated durations are given in Table 3. However the errors in the diffusion times vary depending on the calculation method used. For the algorithm by Petrone et al. (2016), the error ($error_1$ in Table 3) is ±10-62% and for the alternative method proposed here, the error is 10-32%. These errors are separately presented in Table 3. They account for the error in fitting based on analytical scatter and the uncertainty in temperature (±5 °C). With the uncertainty in the activation energy (E_A) and pre-exponential factor (D_0) included (which come with the experimental data on diffusivity, Böhm and Schmidt 2013), the error values ($error_2$ in table 3) increase to 61-288% for the algorithm of Petrone et al. (2016) and to 60-75% for the alternative curve parameter method proposed here.

The effective diffusion times during the experiment (Table 3) are actually a combination of run duration and diffusion while heating and cooling. We use a new approach in which we analytically estimate the possible additional diffusion during heating and quenching. The heating and cooling rates for the experiments are known and for such a case, an effective diffusion coefficient for the total duration of heating and cooling can be calculated. Mathematically, the condition is defined as

$$\int_0^t D dt = D_{eff} t \qquad (4)$$

where t is the duration of heating or cooling and D_{eff} is the effective diffusion coefficient for the duration of heating or cooling which is defined as an integral of the varying diffusion coefficient over time. This is similar to the mathematical concept behind NIDIS model (described earlier). D_{eff}, for a constant rate of heating/cooling can be expressed as (Wilson 1970)

$$D_{eff} = \frac{1}{t}\left(\frac{D_1 {T_1}^2}{\alpha q} - \frac{D_2 {T_2}^2}{\alpha q}\right) \qquad (5)$$

Where T_1 is the final temperature, T_2 is the initial temperature, q is E_A/R, α is the rate of change in temperature, D_1 and D_2 are the diffusion coefficients in the phonolitic melt at T_1 and T_2. We take the lower limit of the temperature range for D_{eff} to be the glass transition temperature for this melt composition (550 °C; Albert 2012), below which diffusion is negligible and the upper limit to be the experimental temperature. Studies by Albert (2012) suggest a glass transition temperature (T_g) of 575-600 °C for the halogen free phonolite melt with 2000-3000 ppm H_2O. 0.4 wt% Cl will not affect the T_g much, while 0.4 wt% F will further reduce Tg by about 15-20 °C (Baasner et al. 2013). Thus, we take the T_g to be 550 °C. In this calculation, we extrapolate the diffusion coefficients down to 550 °C by assuming an Arrhenius relationship between temperature and diffusion coefficient to continue down to 550 °C. Using this extrapolation, we estimated an imaginary effective diffusion profile for heating up to 1200 °C and obtained a similar diffusion length (~0.05 mm for Cl) as for the profiles obtained by Böhm and Schmidt (2013) for their zero time experiment (for heating up to 1200 °C). This suggests that the extrapolation should be a valid approach. Additionally, the diffusion coefficient for temperatures between 550 and 900 °C would be much lower than that for experimental temperatures of 975 to 1150 °C. Considering this and the duration of heating, which is very short (<8% of experimental time), any small deviation from Arrhenius behavior between 550 and 900 °C would be insignificant at a rate of heating of 40 °C/min and a cooling rate at 150 °C/s. Using the effective diffusion coefficient and the duration of heating/cooling, an equivalent time-scale for the additional diffusion is obtained. This equivalent additional diffusion time is equivalent to the duration of additional diffusion at the experimental temperature and is given by

$$t_{additional} = \frac{D_{eff}.t}{D_{experimental}} \tag{6}$$

where $D_{experimental}$ is the diffusion coefficient during the experimental run-time (calculated using experimental temperature and data from Böhm and Schmidt 2013). The values of D_{eff}, $D_{eff}t$ and $t_{additional}$ are presented in supplementary material 1. The additional diffusion time ($t_{additional}$) is added to the experimental duration to obtain the total effective diffusion time, which is compared against the calculated diffusion times from the diffusion profiles. The additional diffusion time, accounting only for heating, ranges from 78 to 279 seconds (0.022 – 0.077 hours) for all diffusive boundaries of both Cl and F. Rapid quenching, however, accounts for a maximum of only 1 s (0.00034 hours) of additional time. The maximum estimated total additional diffusion that occurred in experimental set 2 (at 1150 °C and total run time for T_1 of 3 hours or 10800 seconds) for F accounts for an extra 0.077 hours or 280 seconds (2.6 %).

Our results (Table 3) show that the estimated diffusion times match well with the actual values of t_1 and t_2 of the experiment. The deviation of calculated values from actual values is between 1.1% and 18.2%. This suggests that the non-isothermal diffusion incremental step model works for crystals with multiple zonation provided the temperature during the growth of each zone is well-constrained and the times of changing temperature is relatively short (less than 8% of total diffusion times). For a case where diffusivity is dependent on other factors e.g. pressure or oxygen fugacity (e.g. Fe-Mg diffusion in olivine, Dohmen and Chakraborty 2007), constraining these factors during the course of the crystal growth will also be necessary to apply the model effectively.

Estimating errors in non-isothermal diffusion modelling:

The maximum observed deviations between calculated and experimental diffusion times for F are 18.2% for capsule 2 of set 2 and 7.8% for capsule 1 of set 3. This is mostly because of the higher scatter in F contents due to the higher analytical uncertainty of the electron microprobe for light elements. The detection limit for F is 180 ppm (compared to 50 ppm for Cl) and the relative standard deviation (at 2σ) for F is ~15% (compared to ~7% for Cl). The scatter in the data points is within the uncertainty of ±15%.

Here we have designed the experiments equivalent to a crystal with only two diffusive boundaries within three growth zones of a crystal. The NIDIS model for calculating diffusion times can be extended to more than two diffusive boundaries following an equivalent algorithm where the calculations start backwards from the outer most rim and end at the core.

To assess the total error on individual diffusion time estimates, the sources of contributing errors need to be constrained. These are the same for both the NIDIS algorithm proposed by Petrone et al. (2016) and the alternative curve parameter method described in this study. However, the algorithm presented by Petrone et al. (2016) does not consider uncertainties in the diffusivity parameters (E_A and D_0). Therefore, in order to allow direct comparison against the algorithm by Petrone et al. (2016), $error_1$ (Table 3) is estimated which deliberately excludes uncertainties in E_A and D_0, as discussed in detail in this section. However, an $error_2$, which includes uncertainties in E_A and D_0, is also estimated, presented separately in Table 3, and discussed later in this section. Here, we use the absolute error values from the curve parameter method to first discuss the major sources and their contribution, and then compare them individually to those from the NIDIS algorithm.

The error due to the uncertainty in temperature is significant in diffusive analysis (Costa and Morgan 2010) because of the exponential relationship between the diffusion coefficient and temperature (Eq 1). In our experiments the uncertainty is up to ±5 °C which accounts for ±3 - 7% error in estimated diffusion times and constitutes up to ~55 % of the total error ($error_1$) . However, in natural samples where the temperature values are estimated using thermometric calculations, uncertainty of ±15-20 °C and more is inevitable. For example, an uncertainty of ±20 °C during Cl and F diffusion in phonolite melt will transfer into an error of 15-27% in calculated diffusion times. For elements with higher activation energy (e.g. Ba and Sr; Cherniak 2010), the error can be up to 70% for a temperature of 1000 °C. Petrone et al. (2016) applied their NIDIS model to Fe-Mg diffusion in clinopyroxene and report an error of 35-40% in total residence time estimates for a temperature uncertainty of 10-15 °C. The propagated error (at 95% confidence level) in the first step of diffusion is even higher (60-100%). The error decreases by more than 50-70% if the uncertainty in temperature is ignored. Thus, precisely constraining the different temperatures turns out to be the most vital requirement for applying non-isothermal diffusive analysis (Petrone et al. 2016).

A second source of error is the error in curve fitting which contributes significantly to the total error as well. In our measurements, the error due to curve fitting accounts for ~45-80% of the total error (error$_1$). Although this can be reduced with more precise analytical techniques, even small percentages of error can accumulate to give a significantly large error as we go backwards from rim to core in the NIDIS modelling approach. For example, using a simple error propagation method in analyses of 3 diffusive boundaries, each with 20% error in curve fitting, we get a propagated error of 40% in the diffusion time for the inner-most boundary. Thus, it is essential to consider the propagation of error in the application of the NIDIS model. However, the propagation of error can be reduced significantly if we apply the alternative curve parameter method. In that case, for each diffusive boundary, the curve parameter for that boundary will be subtracted by that of the next boundary and the result will be used to estimate the specific time-scale. For each step of calculation, only 2 curve parameters will be involved and the errors from the rest of the boundaries will not have an effect. This will lower the uncertainty in individual diffusion time calculations and eventually in the total diffusion time. For instance, in the example above, every individual diffusion time calculated (except for the outer-most boundary) will have a lower error of only ~28%. This is in contrast to the NIDIS algorithm given by Petrone et al. (2016), where the time-scales from all the previously (starting from rim) analyzed diffusion boundaries are used to estimate the diffusion time for a particular boundary.

Another advantage of the curve parameter method over the algorithm given by Petrone et al. (2016) is that the contribution of uncertainty in temperature to the error in individual (except for the outer most) and total diffusion time is significantly limited. If we take for example a crystal with 2 diffusive boundaries, then for the core-mantle boundary, t_1 is obtained as $(CP_1 – CP_2)/D_1$. In this case, the uncertainty in temperature contributes only once through D_1 (which is obtained using T_1). This stays true even for a crystal with multiple number of diffusive boundaries where $t_n = (CP_n – CP_{n+1})/D_n$. Conversely, the algorithm given by Petrone et al. (2016), calculates t_1 as the difference between the imaginary time-scales t_3 and t_4, both of which are calculated from each of the two fitting parameters ($\sqrt{4Dt}$ from curve fitting) using D1 individually. In that case, the uncertainty in temperature contributes twice to the error in calculated diffusion time.

To demonstrate the differences between the two algorithms, we calculated the diffusion times for the halogen profiles also using the algorithm by Petrone et al. (2016). The error obtained is 60-100% higher for Cl and 20-51% higher for F in values of t_1 compared to the error obtained using our new alternative algorithm (Table 3). The error in the total time scales was also increased by 28-94% for Cl and 14-30% for F. Except for the error in t_1 and t, the values for t_1, t_2 and t are the same in both the methods, which is expected as both the methods are mathematically consistent. The errors for t_2 are also the same as both the methods use a basic curve fitting of the rim-mantle boundary and D_2 to obtain t_2. The difference in errors is higher for Cl compared to F because Cl has a higher activation energy (153 kJ/mol) compared to F (99.8 kJ/mol) (Böhm and Schmidt 2013). A higher activation energy will yield a higher total fraction of error (see Appendix 1).

We used the data given by Petrone et al. (2016) for multiple zoned clinopyroxene crystals from Stromboli volcano (Italy) to re-estimate the diffusion time with our new algorithm. The results (Table 4) show that the curve parameter method yields 26-40% error (2σ) in t_1 compared to the original 61-100% error (2σ) given by Petrone et al. (2016). The error in the total diffusion time is also slightly less (33-38% compared to 36-40%). The difference in the error in the total diffusion time is less because the difference only occurs in t_1, which in this case, is very small (only 1/10 to 1/4 of t_2). As the error in t_2 remains the same from both the methods and because t_2 is much longer than t_1, the total error does not change much in this case, although the difference is very large for t_1. However, the value of the non-isothermal diffusion model lies in its ability to estimate t_1 and thus, the error in t_1 is extremely vital and should be minimized. These differences in the error in diffusion time are for a temperature uncertainty of 15 and 10 °C as reported by Petrone et al. (2016) at 1098 and 1150 °C respectively. The difference in the error obtained by both the methods will be even higher for temperature values with higher uncertainty and/or for elements with higher activation energies for diffusion.

A third source of uncertainty is the uncertainty associated with diffusivity parameters (activation energy E_A and pre-exponential factor D_0). These come directly from experimentally determined data and are generally unavoidable. We use the uncertainties given by Böhm and Schmidt (2013) (~7.5 kJ/mol in E_A and 1.2×10^{-8} - 1.3×10^{-7} m^2/s in D_0 for both F and Cl). When included, it can constitute up to 57-84% of the total error ($error_2$ in Table 3). Petrone et al. (2016), however, had not considered this source of error. To analyze the difference between the two algorithms, we incorporated this uncertainty into the algorithm by Petrone et al. (2016) and estimated the error on the diffusion times in our samples. The difference between the errors from the curve parameter and the algorithm by Petrone et al. (2016) is even higher, when uncertainties in E_A and D_0 are included. The curve parameter method yields only 60-75% error in contrast to 61-288% of the NIDIS algorithm by Petrone et al. (2016). This is because, like temperature, the contributions of uncertainties in E_A and D_0 are limited to only once in the curve parameter method, whereas in the algorithm by Petrone et al. (2016), they contribute to the error in each imaginary duration individually, thus contributing more than once to every diffusion time (except for the outer-most boundary).

Another source of uncertainty is the rate of temperature change between, and within distinct diffusion intervals. The present non-isothermal diffusion model assumes that temperature follows an ideal step function with (1) negligible periods of temperature change and (2) constant temperatures between the temperature changes. The assumption of constant temperature between temperature changes is hardly applicable for natural samples where, after a sharp heating event, the temperature may again decrease slowly due to cooling until the next heating event occurs. Such a saw tooth pattern in the temperature history is indeed evident in crystals that had long storage times and underwent growth and resorption (for examples see Cooper and Kent 2014; Rubin et al. 2017; Ginibre et al. 2007). Moreover, the assumption of instantaneous temperature change might also not always be valid. For example, for strong and short heating events (like in the models by Cooper and Kent 2014; Rubin et al. 2017; Ginibre et al. 2007), although the short duration of heating might be negligible for long duration of diffusion of slow elements like Ba and Sr (Cherniak 2010), it will be significant for short duration of diffusion of faster elements. For example, a fast diffusing element like Li (8-9 orders of magnitude faster than Ba and Sr in feldspars, Cherniak 2010) in a rapidly evolving, high-temperature mafic system with very short crystal residence times (weeks to months) will be affected even by heating intervals as short as a few days. This can also be seen in the calculated additional diffusion times (supplementary material 1) accounting for the time the samples spent during heating and quenching in our experiment. These additional times for F are ≥2 times higher than those of Cl for the exact same duration of heating and quenching. Such scenarios will make the assumption of (1) isothermal periods between (2) instantaneous temperature change invalid. In such complicated cases, the non-isothermal incremental step model can still be applied, however, for the modeling of individual diffusion boundaries, the changes in temperature variations during the diffusion process also need to be taken into account. This can be achieved using effective diffusion coefficients (Eq. 4 and Eq. 5) and following the same procedure (described earlier) as used to estimate the extra time accounting for additional diffusion during heating and quenching, if the cooling or heating rate is well-constrained. However, for most cases, especially in silicic systems, where crystal residence lasts for thousands to hundreds of thousands of years (Morgan and Blake 2006), short periods of heating (up to a few years) would be insignificant. Secondly, for most cases where magmatic differentiation is interrupted by recharge events, the temperature differences between distinct growth zones will be much larger than the temperature variation during growth between the abrupt events of temperature change. In these cases, the regular non-isothermal incremental step model can still be efficient in extracting the pre-eruptive history of a growing magmatic crystal.

Application to other natural samples:

We are not aware of published studies that would allow to further test the non-isothermal modeling due to (1) lack of individual temperature data for different growth and diffusion intervals of the crystals (e.g. Zellmer et al. 1999; Costa et al. 2003; Zellmer and Clavero 2006; Chamberlein et al. 2014) and (2) lack of (or lack of data on) multiple zone boundaries (e.g. Costa et al. 2003; Chamberlein et al. 2014; Costa and Dungan 2005; Costa and Chakraborty 2004; Ackerson et al. 2018; Iovine et al. 2017).

Therefore, we demonstrate such a test based on our own data on a sanidine megacryst (Fig 4) from a Late Pleistocene to Holocene eruption stage (0.45 Ma – present; Clavero et al. 2004b) of Taapaca volcano (N. Chile). Zellmer and Clavero (2006) applied isothermal diffusion analysis to a similar sanidine megacryst from this volcano and estimated diffusion times ranging from 0.5 to 1.3 ky. Such sanidine megacrysts, present in every eruption stage of Taapaca volcano, are compositionally and texturally very similar (Banaszak 2014). This allows us to analyze one of the megacrysts for non-isothermal diffusion modeling and compare the results to isothermal analysis (Zellmer and Clavero 2006).

The analyzed megacryst (Fig 4) consists of 3 significant Ba-zonations separated by resorption surfaces, which are ideal to apply diffusion chronometry as they ensure an initial sharp compositional profile to start with. Each zone contains amphibole and plagioclase inclusions (Fig 4a) that allow to constrain the temperature during the growth of each zone. We applied the thermometer given by Ridolfi et al. (2010) to the amphibole inclusions and obtained temperatures between 787 and 830 °C. After verifying an apparent linear relationship between grey-scale values from BSE images and Ba-content (Fig 4e, further details in supplementary material 2) in the crystal, we used grey-scale values as proxy for Ba-content and extracted grey-scale profiles (Fig 4b, c and d) to be used for Ba-diffusion modeling. The data for this analysis are given in supplementary material 2. We used the Ba diffusivity data given by Cherniak (2002) (Ea=455000 J/mol and D_0=0.29 m^2/s) and applied the non-isothermal diffusive analysis (both NIDIS algorithm and curve parameter method). For comparison we also modeled the profiles for isothermal diffusion at 787 and 830 °C, the minimum and the maximum temperatures obtained from thermometry.

The calculated diffusion times are presented in Table 5. It is evident that the non-isothermal diffusion, which takes temperature specific to each zone into account, returns significantly different individual and total diffusion times compared to isothermal calculation. The diffusion times of 1.5 – 9.4 ky are also different from the isothermal diffusion times of 0.5-1.3 ky obtained by Zellmer and Clavero (2006) at 875 °C. If they had used a more realistic albeit constant temperature value, e.g. between 787 and 830°C, their diffusion time estimate would have been much longer. It is also evident that, as shown earlier, although both the curve parameter method and the NIDIS algorithm obtain the same diffusion times, the curve parameter method returns a significantly lower error (67-108%) compared to the original NIDIS algorithm of Petrone et al. (2016) (100-352%). Apart from the accuracy of curve parameter method, this analysis shows that if the temperature-time history across several growth and diffusion zones can be constrained, the non-isothermal analysis gives more robust and significantly different total diffusion time-scale compared to traditional isothermal analysis.

Implications

As argued above, the non-isothermal diffusion modeling of magmatic crystals with multiple diffusion interfaces at multiple resorption interfaces should result in more realistic diffusion and residence time estimates revealing valuable information for complexly zoned crystals, provided the temperature is properly constrained. For example, Petrone et al. (2016) inferred from the model that the Stromboli magma system is a well-mixed reservoir where the inputs of fresh magma are rapidly (within ~1-2 years) homogenized within the resident magma. Such detailed information cannot be extracted using isothermal diffusive analysis. Our own analysis of the Taapaca sanidine megacryst also shows that the non-isothermal diffusion model provides more reliable information for crystals that show highly complex zonation and resorption patterns with respect to total diffusion times, crystal residence times and the history of magmatic process prior to eruption.

However, the potential pitfalls due to accumulating effects of errors and insufficient precision on constrained temperature histories and not-so-perfect curve-fitting must be realized. This limits the use of the modified NIDIS model to only a few well-constrained cases where T-t history can be constrained.

The increased focus on methods of geothermo- and barometry in magmatic systems (e.g. Putirka 2008; Ridolfi et al. 2010; Mutch et al. 2016; Sun and Liang 2017; Reverdatto et al. 2019) should improve and enable us to use the non-isothermal diffusion in future studies. The improved assessment of errors in this study provides detail on the extent to which major errors (e.g. due to temperature uncertainty, curve fitting and diffusivity data) can propagate and how to minimize them. Considering errors realistically is necessary to use the model, for natural systems and to constrain the validity, advantages and limitations of the non-isothermal diffusion. Beyond the application to zoned crystals in magmatic systems, the improved approach to the NIDIS algorithm can also be applied to diffusional mass transport processes in general, as the underlying principle will remain the same.

Acknowledgements

This study is a part of the doctoral research project funded by a scholarship from Deutscher Akademischer Austauschdienst (DAAD) to S. S. Rout. We thank A. Kronz for his support during electron microprobe analysis and B. Schlieper-Ludewig for her assistance during the initial glass preparation. We also appreciate the effort of D. Baker (editor), C Lesher (associate editor) and two anonymous reviewers whose comments and suggestions have helped in improving the manuscript.

References

Ackerson, M.R., Mysen, B.O., Tailby, N.D., and Watson, E.B. (2018) Low-temperature crystallization of granites and the implications for crustal magmatism. Nature, 559, 94-97.

Albert, C. (2012) Experimentelle Bestimmung der Viskosität wasserhaltiger Phonolithschmelzen, Diploma thesis, Georg-August Universität, Göttingen (in German).

Alletti, M., Baker, D.R., and Freda, C. (2007) Halogen diffusion in a basaltic melt. Geochimica et Cosmochimica Acta, 71, 3570–3580.

Baasner, A., Schmidt, B.C., and Webb, S.L. (2013) The effect of chlorine, fluorine and water on the viscosity of aluminosilicate melts. Chemical Geololgy, 357, 134-149.

Balcone-Boissard, H., Baker, D.R., Villemant, B., and Boudon, G. (2009) F and Cl diffusion in phonolitic melts: influence of the Na/K ratio. Chemical Geology, 263, 89–98.

Banaszak, M. (2014) Differentiation regimes in the Central Andean magma systems: case studies of Taapaca and Parinacota volcanoes, Northern Chile, PhD thesis, Georg-August Universität, Göttingen.

Befus, K.S., Watkins, J., Gardner, J.E., Richard, D., Befus, K.M., Miller, N.R., and Dingwell D.B. (2015) Spherulites as in-situ recorders of thermal history in lava flows. Geology, 43, 647–650.

Benne, D., and Behrens, H. (2003) Water solubility in haplobasaltic melts. European Journal of Mineralogy, 15, 803–814.

Bloch, E., and Ganguly, J. (2014) ^{176}Lu–^{176}Hf and ^{147}Sm–^{143}Nd ages of the Martian shergottites: Evaluation of the shock-resetting hypothesis through diffusion kinetic experiments and modeling, and petrological observations. Earth and Planetary Science Letters, 395, 173-183.

Böhm, A., and Schmidt, B.C. (2013) Fluorine and chlorine diffusion in phonolitic melt. Chemical Geology, 346,162-171.

Chakraborty, S. (2008) Diffusion in solid silicates: a tool to track timescales of processes comes of age. Annual Review of Earth and Planetary Sciences, 36, 153–190.

Chamberlain, K.J., Morgan, D.J., Wilson, C.J.N. (2014) Timescales of mixing and mobilisation in the Bishop Tuff magma body: perspectives from diffusion chronometry. Contributions to Mineralogy and Petrology, 167, 1034.

Cherniak, D.J. (2002) Ba diffusion in feldspar. Geochimica et Cosmochimica Acta, 66, 1641-1650.

Cherniak, D.J. (2010) Cation diffusion in feldspars. In Y. Zhang, and D.J. Cherniak, Eds, Diffusion in Minerals and Melts, 72, p. 691-733. Reviews in Mineralogy and Geochemistry, Mineralogical Society of America and Geochemical Society.

Clavero, J.E., Sparks, R.S.J., Pringle, M.S., Polanco, E., and Gardeweg, M. (2004b.) Evolution of Taapaca Volcanic Complex, Central Andes of Northern Chile. Journal of the Geological Society, 161, 603–618.

Condomines, M., Hemond, C., and Allegre, C.J. (1988) U–Th–Ra radioactive disequilibria and magmatic processes. Earth and Planetary Science Letters, 90, 243–262.

Cooper, K.M., Reid, M.R., Murrell, M.T., and Clague, D.A. (2001) Crystal and magma residence times at Kilauea Volcano, Hawaii: ^{230}Th-^{226}Ra dating of the 1955 east rift eruption. Earth and Planetary Science Letters, 184, 703-718.

Cooper, K.M., and Kent, A.J.R. (2014) Rapid remobilization of magmatic crystals kept in cold storage. Nature, 506, 480-483.

Costa, F., and Chakraborty, S. (2004) Decadal time gaps between mafic intrusion and silicic eruption obtained from chemical zoning patterns in olivine. Earth and Planetary Science Letters, 227, 517-530.

Costa, F., Chakraborty, S., and Dohmen, R. (2003) Diffusion coupling between trace and major elements and a model for calculation of magma residence times using plagioclase. Geochimica et Cosmochimica Acta, 67, 2189-2200.

Costa, F., Dohmen, R., and Chakraborty, S. (2008) Time scales of magmatic processes from modelling the zoning patterns of crystals. In K.D. Putirka and F.J. Tepley, III, Eds, Minerals, Inclusions and Volcanic Processes, 69, p. 545-594. Reviews in Mineralogy and Geochemistry, Mineralogical Society of America and Geochemical Society.

Costa, F., and Dungan, M. (2005) Short time scales of magmatic assimilation from diffusion modeling of multiple elements in olivine. Geology, 33, 837–840

Costa, F., and Morgan, D. (2010) Time constraints from chemical equilibration in magmatic crystals. In A. Dosseto, S.P. Turner and J.A. Van Orman, Eds, Timescales of magmatic processes: from core to atmosphere. John Wiley & Sons, Ltd, Chichester, UK. doi: 10.1002/9781444328509.ch7

Crank, J. (1975) The Mathematics of Diffusion. Clarendon-Oxford, London.

Dingwell, D.B., and Scarfe, C.M. (1984) Chemical diffusion of fluorine in jadeite melt at high pressure. Geochimica et Cosmochimica Acta, 48, 2517–2525.

Dohmen, R., and Chakraborty, S. (2007) Fe–Mg diffusion in olivine II: point defect chemistry, change of diffusion mechanisms and a model for calculation of diffusion coefficients in natural olivine. Physics and Chemistry of Minerals, 34, 409–430.

Ganguly, J., Dasgupta, S., Cheng, W., and Neogi, S. (2000) Exhumation history of a section of the Sikkim Himalayas, India: records in the metamorphic mineral equilibria and compositional zoning of garnet. Earth and Planetary Science Letters, 193, 471-486.

Gardner, J.E., Befus, K.S., Watkins, J., Hesse, M., and Miller, N. (2012) Compositional gradients surrounding spherulites in obsidian and their relationship to spherulite growth and lava cooling. Bulletin of Volcanology, 74, 1865-1879.

Ginibre, C., Wörner, G., and Kronz, A. (2004) Structure and Dynamics of the Laacher See Magma Chamber (Eifel, Germany) from Major and Trace Element Zoning in Sanidine: a Cathodoluminescence and Electron Microprobe Study. Journal of Petrology, 45, 2197–2223.

Ginibre, C., Wörner, G., and Kronz, A. (2007) Crystal zoning as archives for magma evolution. ELEMENTS, 3, 261-166.

Hawkesworth, C.J., Blake, S., Evans, P., Hughes, R., Macdonald, R., Thomas, L.E., Turner, S.P., and Zellmer, G. (2000) Time scales of crystal fractionation in magma chambers-integrating physical, isotopic and geochemical perspectives. Journal of Petrology, 41, 991–1006.

Hawkesworth, C., George, R., Turner, S., and zellmer, G. (2004) Time scales of magmatic processes. Earth and Planetary Science Letters, 218, 1-16.

Holland, T., and Blundy, J. (1994) Non-ideal interactions in calcic amphiboles and their bearing on amphibole- plagioclase thermometry. Contributions to Mineralogy and Petrology, 116, 433-447.

Iovine, R.S., Fedele, L., Mazzeo, F.C., Arienzo I., Cavallo, A., Wörner G., Orsi, G., Civetta, L., and D'Antonio, M. (2017) Timescales of magmatic processes prior to the ~4.7 ka Agnano-Monte Spina eruption (Campi Flegrei caldera, Southern Italy) based on diffusion chronometry from sanidine phenocrysts, Bulletin of Volcanology, 79, 18.

Johnson, M.C., and Rutherford, M.J. (1989) Experimental calibration of the aluminum-in-hornblende geobarometer with application to Long Valley caldera (California). Geology, 17, 837-841.

Lasaga, A. (1983) Geospeedometry: an extension of geothermometry. In S.K. Saxena, Eds, Kinetics and Equilibrium in Mineral Reactions, 2, p. 81-114. Advances in Physical Geochemistry, Springer, New York.

Morgan, D.J., and Blake, S. (2006) Magmatic residence times of zoned phenocrysts: introduction and application of the binary element diffusion modelling (BEDM) technique. Contributions to Mineralogy and Petrology, 151, 58-70.

Morgan, D.J., Blake, S., Rogers, N.W., DeVivo, B., Rolandi, G., Macdonald, R., and Hawkesworth C.J. (2004) Time scales of crystal residence and magma chamber volumes from modelling of diffusion profiles in phenocrysts: Vesuvius 1944. Earth and Planetary Science Letters, 222, 933–946.

Mutch, E.J.F., Blundy, J.D., Tattitch, B.C., Cooper, F.J., and Brooker R.A. (2016) An experimental study of amphibole stability in low-pressure granitic magmas and a revised Al-in-hornblende geobarometer. Contributions to Mineralogy and Petrology, 171, 85.

Petrone C.M., Bugatti, G., Braschi, E., and Tommasini, S. (2016) Pre-eruptive magmatic processes re-timed using a non-isothermal approach to magma chamber dynamics. Nature communications, 7, 12946.

Putirka, K. (2008) Thermometers and Barometers for Volcanic Systems. In K. Putirka and F. Tepley, Eds, Minerals, Inclusions and Volcanic Processes, 69, p. 61-120. Reviews in Mineralogy and Geochemistry, Mineralogical Society of America and Geochemical Society.

Reid, M.R. (2003) Timescales of magma transfer and storage in the crust. In R.L. Rudnick, Ed, The Crust, Treatise on Geochemistry 3, p. 167-193. Elsevier, Oxford.

Reverdatto, V.V., Likhanov, I.I., Polyansky, O.P., Sheplev, V.S., and Kolobov, V.Y. (2019) Mineral Geothermobarometry. In The Nature and Models of Metamorphism. Springer Geology. Springer, Cham.

Ridolfi, F., Renzulli, A., and Puerini, M. (2010) Stability and chemical equilibrium of amphibole in calc-alkaline magmas: an overview, new thermobarometric formulations and application to subduction-related volcanoes. Contributions to Mineralogy and Petrology, 160, 45-66.

Roux, J., and Lefèvre, A. (1992) A fast-quench device for internally heated pressure vessels. European Journal of Mineralogy, 4, 279–281.

Rubin, A.E., Cooper, K.M., Till, C.B., Kent, A.J.R., Costa, F., Bose, M., Gravley, D., Deering, C., and Cole, J. (2017) Rapid cooling and cold storage in a silicic magma reservoir recorded in individual crystals. Science, 356, 1154-1156.

Ruprecht, P., and Wörner, G. (2007) Variable regimes in magma systems documented in plagioclase zoning patterns: El Misti stratovolcano and Andagua monogenetic cones (S. Peru). Journal of Volcanology and Geothermal Research, 165, 142-162.

Saal, A.E., Hauri, E.H., Lo Cascio, M., Van Orman, J.A., Rutherford, M.C., and Cooper, R.F. (2008) Volatile content of lunar volcanic glasses and the presence of water in the Moon's interior. Nature, 454, 192–196

Schmitt, A.K. (2011) Uranium series accessory crystal dating of magmatic processes. Annual Review of Earth and Planet Sciences, 39, 321-349.

Sun, C., and Liang, Y. (2017) A REE-in-plagioclase-clinopyroxene thermometer for crustal rocks. Contributions to Mineralogy and Petrology, 172, 24.

Watson, E.B., and Müller, T. (2009) Non-equilibrium isotopic and elemental fractionation during diffusion-controlled crystal growth under static and dynamic conditions. Chemical geology, 267, 111-124.

Wilson, P.R. (1970) A solution to the diffusion equation for non isothermal diffusion. Solid-State Electronics, 13, 1311–1313.

Zellmer, G.F., Blake, S., Vance, D., Hawkesworth, C., and Turner, S. (1999) Short plagioclase residence times at two island arc volcanoes (Kameni islands, Santorini, and Soufriere, St. Vincent) determined by Sr diffusion systematics. Contributions to Mineralogy and Petrology, 136, 345-357.

Zellmer, G.F., and Clavero, J.E. (2006) Using trace element correlation patterns to decipher a sanidine crystal growth chronology: An example from Taapaca volcano, Central Andes. Journal of Volcanology and Geothermal Research, 156, 291-301.

Zellmer, G., Turner, S., and Hawkesworth, C. (2000) Timescales of destructive plate margin magmatism: new insights from Santorini, Aegean volcanic arc. Earth and Planetary Science Letters, 174, 265-281.

Figure captions

Fig 1: Schematic diagram that explains the model and the steps of the experiment. (a) At t=0 and $T=T_1$, the mantle is formed. The compositional profile across the core-mantle boundary at this point is an initial step function. The equivalent step in the experiment is the start of the experiment where capsule 1 is heated to T_1 and diffusion begins. (b) diffusion continues at $T=T_1$ across the core-mantle boundary and the compositional profile is gradually smoothened out. (c) At $t=t_1$, temperature is changed to T_2 and the rim of the crystal is formed. The mantle-rim compositional profile at this stage is a sharp step function. In the experiment, capsule 2 is added to the system that mirrors mantle-rim boundary. (d) At $t=t_2$ ($t_2>t_1$), closure of diffusion occurs. By this stage, the core-mantle boundary has undergone diffusion for t_1 time at T_1 temperature, then again for t_2 time at T_2 temperature where the mantle-rim boundary has undergone diffusion only for t_2 time at T_2 temperature. In the experiment, this is the stage where the samples are rapidly quenched and closure of diffusion occurs.

Fig. 2: (a) Example of an experimental set (set 2); quenched samples in epoxy, polished and prepared for EMP. (b) Example of a quantitative line analysis (beam diameter 20 µm) across a diffusion interface (BSE image of capsule 1 of set 2). The initial interface between the two glass blocks is marked by a linear array of bubbles which are formed because of the minuscule amount of trapped air between the polished surfaces of the two initial glass blocks.

Fig. 3: Halogen diffusion profiles obtained by EMP from the capsules set 3 of experiments. (a) Cl and (c) F (wt%) profiles in capsule 1 of the experimental set that represents the core-mantle boundary. (b) Cl and (d) F (wt%) profiles in capsule 2 of the experimental set that represents the mantle-rim boundary. The solid red lines are the calculated model curves used for fitting.

Fig. 4: (a) BSE image of the analyzed sanidine megacryst from Taapaca volcano (N. Chile). The three zones in the megacryst are separated by the three boundaries b, c and d. (b), (c) and (d) are the grey-scale profiles at boundaries b, c and d, respectively. The solid red curves are the modeled diffusion curves obtained through curve fitting. The red squares in (a) denote the areas over which these profiles are taken. (e) Correlation between grey-scale values and Ba-content in the megacryst. Amphibole (Amp) inclusions within the zones in (a) yield (f) temperatures (using thermometer by Ridolfi et al. 2010) specific to each inclusion, thus specific to each zone. The error in the temperature is 1σ.

Table captions

Table 1: Chemical composition of the starting glass of MBP composition obtained using EMP

Table 2: Experimental conditions of all sets of experiments including temperature, pressure, duration or run time and, maximum and minimum halogen content. The run time excludes the durations of heating and cooling.

Table 3: Curve parameters from the concentration profiles, diffusion coefficients, effective duration of diffusion during the experiments and the calculated diffusion times (calculated using the NIDIS algorithm by Petrone et al. (2016), curve parameter method from this study, and diffusivity data from Böhm and Schmidt 2013). The effective duration of diffusion constitutes of the experimental duration and the additional time accounting for the diffusion that happened during heating and cooling. The errors in the calculated diffusion times account for the error in curve fitting and the uncertainty in temperature.

Table 4: Comparison of error in diffusion timescales of the 4 clinopyroxene crystals (from Stromboli volcano, Italy) studied by Petrone et al. (2016) using the alternative curve parameter method from this study against the values given by Petrone et al. (2016). The error in t_1, t_2 and total t, calculated using the method described in this study, comprises of the 2σ in both fitting parameter and temperature as given by Petrone et al. 2016. The crystal cpx1 from Petrone et al. (2016) is not mentioned here as it has only 1 diffusive boundary which reduces it to a normal diffusion analysis and the non-isothermal model is not applicable.

Table 5: Obtained individual and total diffusion times from the sanidine megacryst using isothermal and non-isothermal diffusion modeling. The errors in all the diffusion times are 1σ and comprise of uncertainty in temperature (±22 °C) and errors in curve fitting.

Appendix

The relative error propagation on the time-scale obtained from the modeling of each diffusion profile is calculated as follows:

$$\frac{\sigma_t}{t} = \sqrt{\left\{\left(\frac{E_A}{RT}\right)^2 \left[\left(\frac{\sigma_{E_A}}{E_A}\right)^2 + \left(\frac{\sigma_T}{T}\right)^2\right] + \left(\frac{\sigma_{\sqrt{4Dt}}}{\sqrt{4Dt}}\right)^2 + \left(\sigma_{ln|D_0|}\right)^2\right\}} \qquad (7)$$

where t is diffusion time (s), σ_t is the error in diffusion time, E_A is the activation energy, σ_{E_A} is the error in activation energy, R is the universal gas constant, T is the temperature, σ_T is the uncertainty in temperature, D is the diffusion coefficient, $\sigma_{\sqrt{4Dt}}$ is the error in curve fitting, D_0 is the pre-exponential factor and $\sigma_{\ln|D_0|}$ is the uncertainty in $\ln(D_0)$. $\sigma_{\sqrt{4Dt}}$ is the standard error on ‘√(4Dt)’ obtained by using ‘√(4Dt)’ as a single parameter in the curve fitting. For the curve fitting, predefined fitting functions in OriginLab were used which use Chi-Square tolerance value of $1\text{x}10^{-9}$ for an acceptable fit. In the presented results, in error_1, the term σ_{E_A} and $\sigma_{\ln|D_0|}$ are ignored as we compare against the results and algorithm presented by Petrone et al. 2016 who have not considered these errors. However, these are important sources of error that come directly from the experimental data on diffusivity. These uncertainties are included in the total error (Error_2).

Oxides	Wt%	Standard dev. (1σ)
SiO_2	59.08	±0.21
Al_2O_3	18.93	±0.12
Na_2O	10.43	±0.09
K_2O	5.68	±0.04
Fe_2O_3	3.85	±0.06
TiO_2	0.67	±0.03
MnO	0.17	±0.02
MgO	0.32	±0.02
CaO	0.83	±0.03
Total	99.96	

Experiment		Temperature (°C)		Pressure (bar)	Experimental duration/Run time			$C_{halogen}$ max (wt%)		$C_{halogen}$ min (wt%)	
						seconds	hours	Cl	F	Cl	F
Set 1	capsule 1	T_1	1085	1000	t_1	21600	6	0.42	0.39	0.00	0.00
	capsule 1 + capsule 2	T_2	1000	1000	t_2	21600	6	0.41	0.40	0.00	0.00
Set 2	capsule 1	T_1	1150	1000	t_1	10800	3	0.41	0.43	0.00	0.00
	capsule 1 + capsule 2	T_2	1050	1000	t_2	18000	5	0.42	0.38	0.00	0.00
Set 3	capsule 1	T_1	975	1000	t_1	25200	7	0.41	0.38	0.00	0.00
	capsule 1 + capsule 2	T_2	1120	1000	t_2	12600	3.5	0.41	0.40	0.00	0.00

Experiment		CP[a] from profiles (Dt, x10^{-3} mm^2)		CP[a] from each time interval (Dt, x10^{-3} mm^2)			Temperature (° C)	D (x10^{-7} mm^2/s)			Effective time for Cl (hours)		Calculated time for Cl (hours)					Effective time for F (hours)		Calculated time for F (hours)				
													Calculated values	Error						Calculated values	Error			
														CP[a] method		NIDIS algorithm					CP[a] method		NIDIS algorithm	
		Cl	F		Cl	F			Cl	F				Error$_1$[b]	Error$_2$[c]	Error$_1$[b]	Error$_2$[c]				Error$_1$[b]	Error$_2$[c]	Error$_1$[b]	Error$_2$[c]
Set 1	Capsule 1	4.4	68.9	D_1t_1	3.1	44.4	1085	D_1	1.53	20.00	t_1	6.03	5.63	±0.68	±3.54	±1.08	±5.26	t_1	6.07	6.17	±0.85	±3.92	±1.28	±6.36
	Capsule 2	1.3	24.5	D_2t_2	1.3	24.5	1000	D_2	0.61	11.10	t_2	6.02	6.09	±0.74	±3.92	±0.74	±3.92	t_2	6.06	6.13	±0.78	±4.13	±0.78	±4.13
Set 2	Capsule 1	4.9	64.3	D_1t_1	3.1	29.0	1150	D_1	2.78	27.80	t_1	3.04	3.10	±0.39	±1.87	±0.64	±3.12	t_1	3.08	2.90	±0.71	±1.89	±0.90	±4.42
	Capsule 2	1.8	35.3	D_2t_2	1.8	35.3	1050	D_2	1.05	16.40	t_2	5.03	4.76	±0.50	±3.06	±0.50	±3.06	t_2	5.06	5.98	±0.70	±3.87	±0.70	±3.87
Set 3	Capsule 1	3.8	58.0	D_1t_1	1.1	25.1	975	D_1	0.45	9.17	t_1	7.02	6.80	±2.16	±5.11	±4.24	±19.59	t_1	7.05	7.60	±2.41	±5.69	±2.90	±13.84
	Capsule 2	2.7	32.9	D_2t_2	2.7	32.9	1120	D_2	2.14	25.00	t_2	3.54	3.50	±0.34	±2.14	±0.34	±2.14	t_2	3.57	3.65	±0.69	±2.28	±0.69	±2.28

Notes:

[a] CP : Curve parameter, this study.

[b] Error$_1$ is the error calculated excluding the uncertainties in E_A and D_0.

[c] Error$_2$ is the error calculated including the uncertainties in E_A and D_0.

Crystal	Calculated time and errors (yr)											
	t1 (Petrone et al. 2016)	t1 (this study)	error in t1 (2σ, Petrone et al. 2016)	error in t1 (2σ, this study)	t2 (Petrone et al. 2016)	t2 (this study)	error in t2 (2σ, Petrone et al. 2016)	error in t2 (2σ, this study)	total t (Petrone et al. 2016)	total t (this study)	error in total t (2σ, Petrone et al. 2016)	error in total t (2σ, this study)
cpx2	0.2	0.2	0.2	0.05	1.6	1.6	0.6	0.6	1.8	1.8	0.7	0.6
cpx3	0.6	0.6	0.6	0.24	4.2	4.2	1.8	1.8	4.8	4.8	1.9	1.8
cpx4	1.4	1.4	1.2	0.43	9.2	9.2	3.7	3.7	10.6	10.6	3.9	3.6
cpx5*	2.3	2.3	1.4	0.60	9.5	9.5	3.9	3.9	11.8	11.8	4.2	3.9

* for cpx 5 the fitting parameter and 2.s.d. for core-mantle profile was not given by Petrone et al. 2016. Thus for crystal cpx5, we calculated backwards from the presented value of t1 (in Petrone et al. 2016) to obtain corresponding fitting parameter and assummed a 10% 2 s.d. (in line with the mantle-rim profile) and calculated t1 again using the method mentioned in this study.

Zone	T (°C)	Isothermal diffusion time at 787 °C (yr)		Isothermal diffusion time at 830 °C (yr)		Diffusion time NIDIS algorithm (yr)		Diffusion time CP[a] method (yr)		Relative error NIDIS algorithm (%)	Relative error CP[a] method (%)
b	815 ±22	11900	±12800	1.6	±1.6	3.1	±8.6	3.1	±3.2	277	103
c	787 ±22	4800	±5200	0.6	±0.6	4.8	±16.9	4.8	±5.2	352	108
d	830 ±22	11000	±11800	1.5	±1.5	1.5	±1.5	1.5	±1.5	100	100
Total		27700	±18200	3.7	±2.2	9.4	±19	9.4	±6.3	202	67

Notes:

[a] CP: Curve parameter, this study.

Figure 1

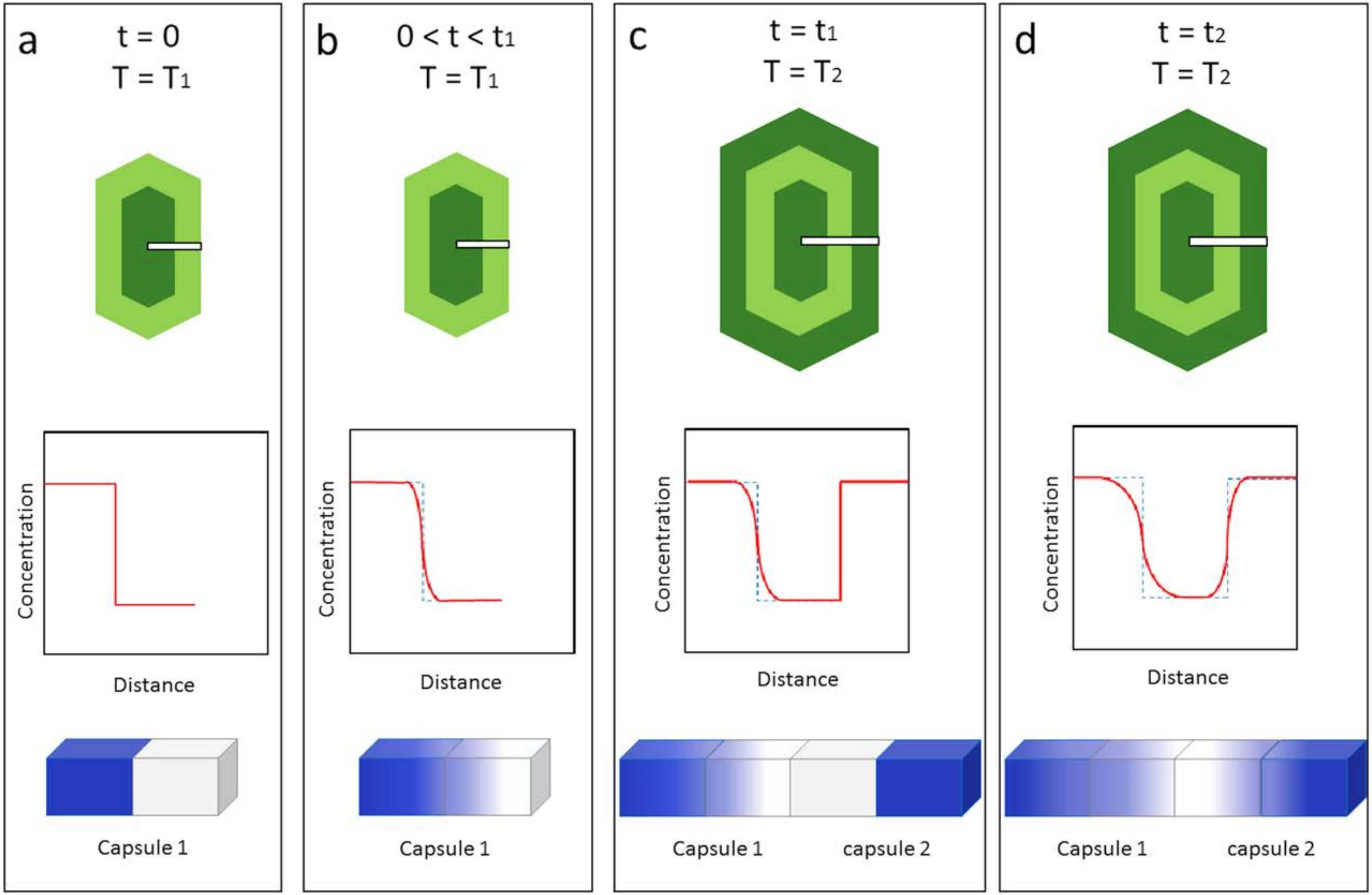
a
t = 0
T = T1
Concentration
Distance
Capsule 1
b
0 < t < t1
T = T1
Concentration
Distance
Capsule 1
c
t = t1
T = T2
Concentration
Distance
Capsule 1
capsule 2
d
t = t2
T = T2
Concentration
Distance
Capsule 1
capsule 2

Figure 2

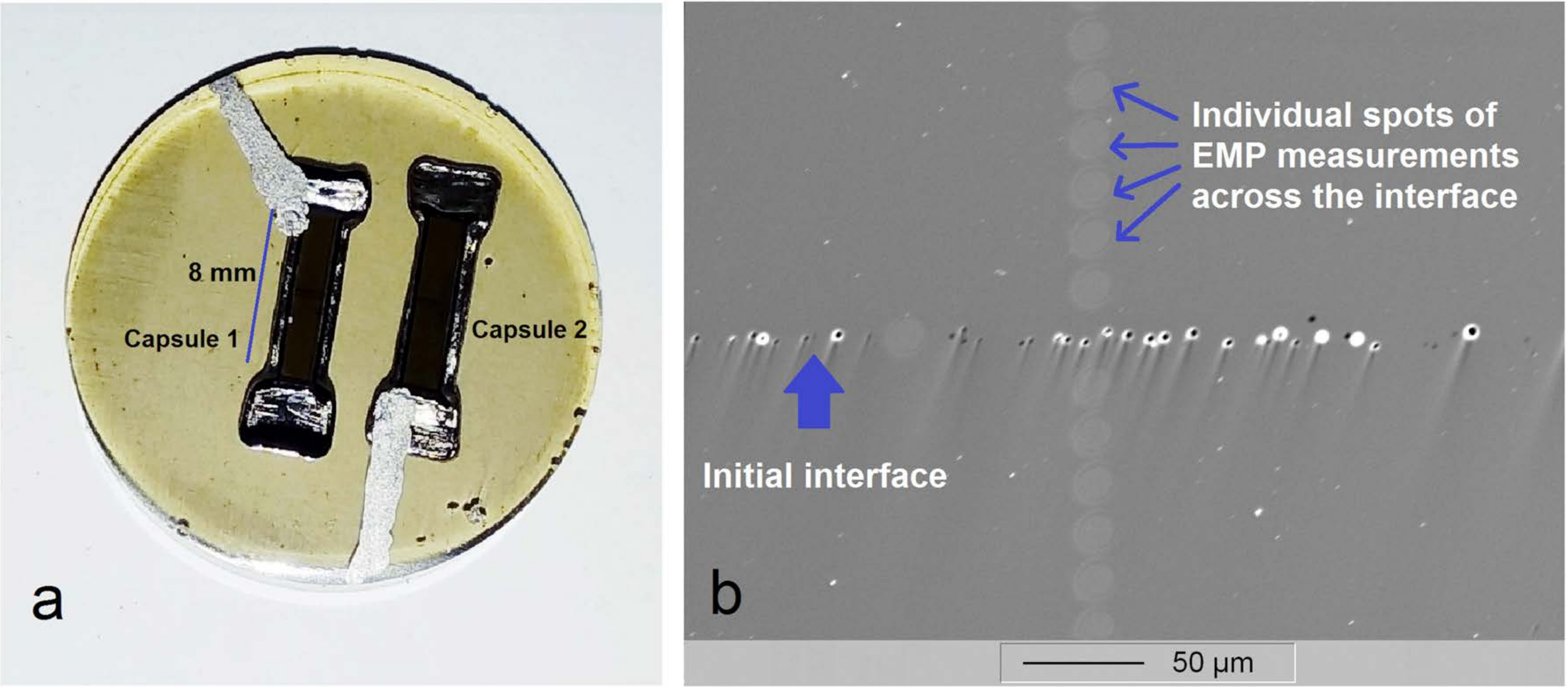
8 mm
Capsule 1
Capsule 2
a
Individual spots of EMP measurements across the interface
Initial interface
b
50 µm

Figure 3

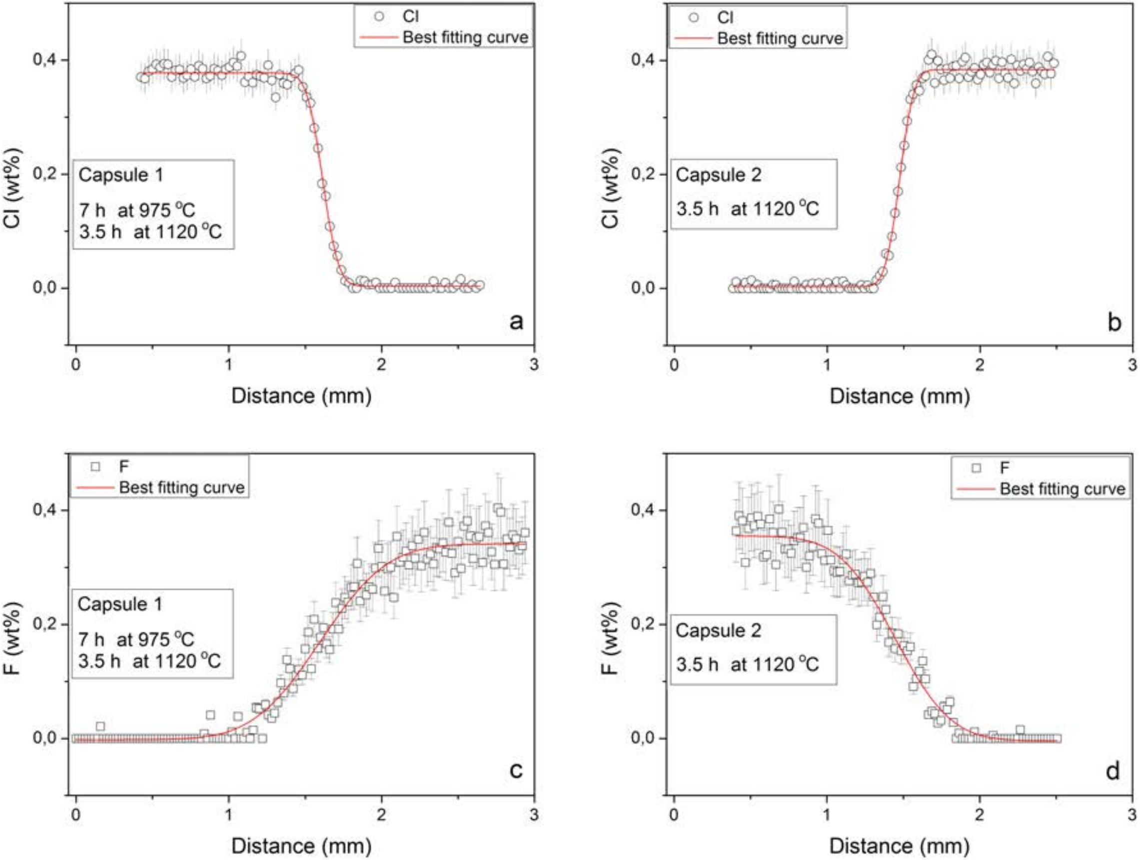

Cl
Best fitting curve
Capsule 1
7 h at 975 °C
3.5 h at 1120 °C
Cl (wt%)
0,4
0,2
0,0
0
1
2
3
Distance (mm)
a
Cl
Best fitting curve
Capsule 2
3.5 h at 1120 °C
Cl (wt%)
Distance (mm)
b
F
Best fitting curve
Capsule 1
7 h at 975 °C
3.5 h at 1120 °C
F (wt%)
Distance (mm)
c
F
Best fitting curve
Capsule 2
3.5 h at 1120 °C
F (wt%)
Distance (mm)
d

Figure 4

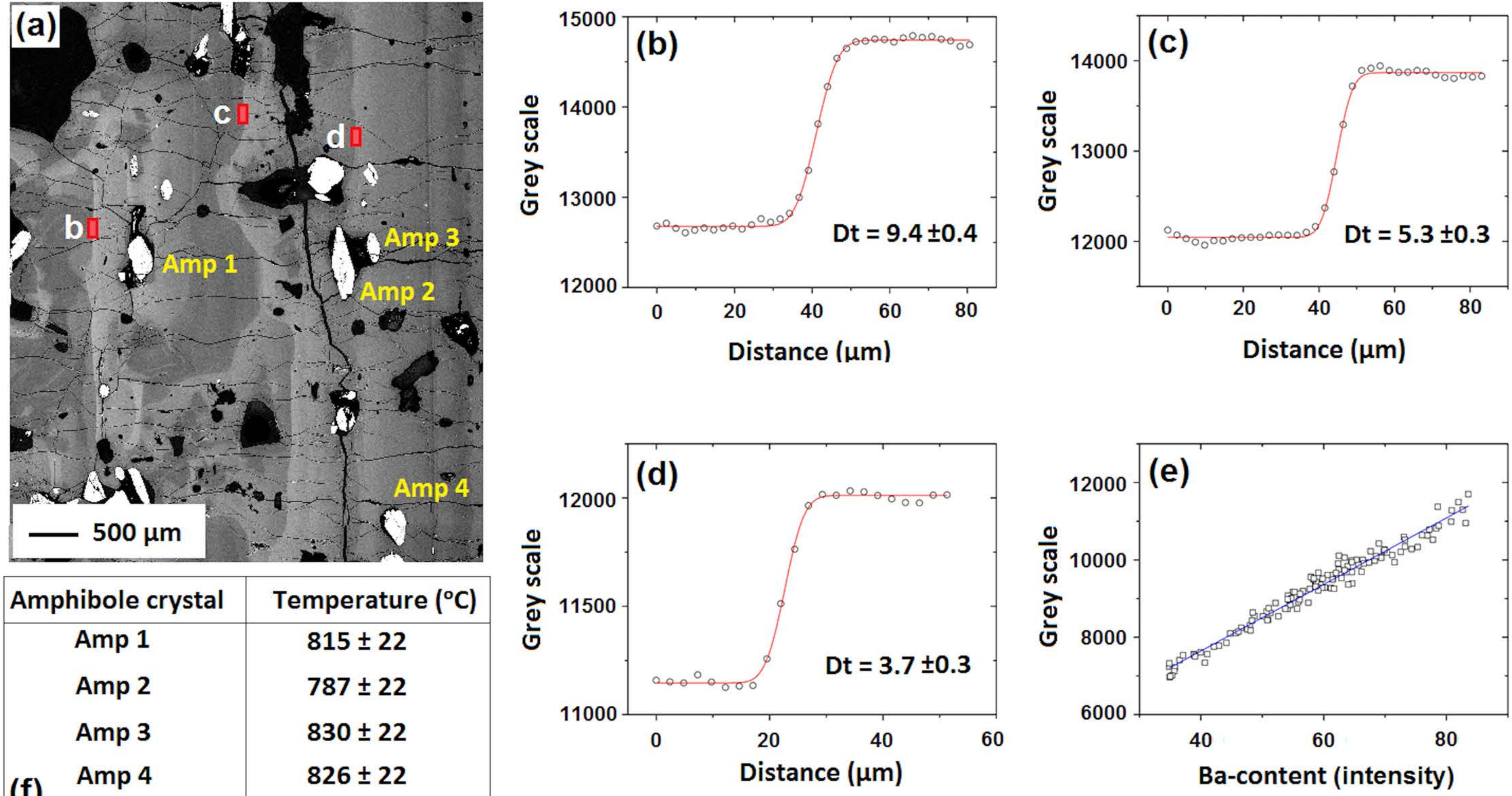

Amphibole crystal	Temperature (°C)
Amp 1	815 ± 22
Amp 2	787 ± 22
Amp 3	830 ± 22
Amp 4	826 ± 22

(f)